

# Quantum Sensing on a Classical Budget: Towards Industrially Viable Self-Mixing Interferometry

Stefan Martin, Trevor J. McCourt, Jeremy Newton, Alexandra Mihaila

Self-Mixing Interferometry (SMI) is a laser measurement technique that leverages interference at the laser source. Commonly implemented using inexpensive semiconductor diode lasers, this method is able to perform displacement measurements at the wavelength scale. There has been substantial research into the technology over the last two decades, and an increasing number of complicated and accurate configurations have been developed that are useful in general metrology scenarios. Instead of pushing for higher performance in general, here we instead focus on understanding, characterizing, and finding applications for a very simple and cheap SMI architecture that can be built for approximately \$100. Most notably, we measure a diode temperature dependence that aligns closely with theoretical expectations and report on a method to achieve extreme sensitivity by biasing the sensor towards its critical point when operating in the moderate-coupling regime. This suggests that simple, robust SMI sensors that are several orders of magnitude cheaper than competing solutions may be usable in very specific industrial applications.

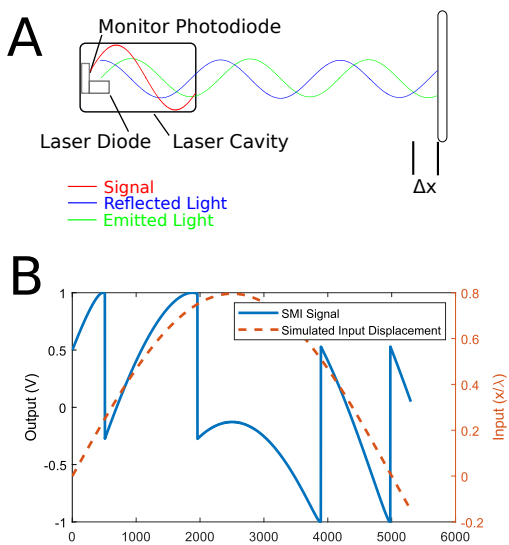


Figure 1. A) The basic mechanism of self-mixing interferometry in which a laser is bounced off of the target back into the laser cavity where the interference between the emitted and reflected beams is measured by an integrated photodiode. B) A simulated SMI signal in the moderate coupling regime showing the fringe structure.

## I. INTRODUCTION

Self-mixing interferometry is a method of laser measurement which operates via the interference of a beam which has been backscattered into the laser source by a remote target. This method of interferometry differs drastically from conventional configurations as it does not employ a reference arm and can thus be implemented with very inexpensive optics. The signal measured by this interferometer is an amplitude modulated current generated by a photodetector measuring the resultant op-

tical power created by the superposition of the backscattered beam and the reverse emission of the laser.

The components of the most basic SMI system are a single-mode laser with a photodetector to measure the mixed signal, a single aspheric collimating lens, an attenuator to control the coupling regime, and a reflective target which couples the laser back into itself to form the external cavity. This configuration was first implemented with a HeNe laser by [1]. The measurement process can be simplified greatly by the use of GaAs diode lasers with integrated photodiodes, and was first demonstrated by [2]. SMI setups based on visible laser diodes are attractive due to their extremely low cost and will be the primary focus of this paper.

The SMI mechanism can be explained by the physics of a compound-cavity laser [3]. In SMI systems an external cavity is formed between the reflective target and the emission window of the laser. When the optical path length of this external cavity is less than the coherence length, interference will occur between the backscattered beam and that emitted by the laser. This optical configuration is sensitive to changes in the position of the target since any change to the length of the external cavity will alter the resonant modes possible within it. A displacement of the reflective target has been shown to impart both an amplitude and a wavelength modulation in the cavity field which can be measured at any point in the laser path [1]. As shown in 1, these modulations have components of  $\sin 2kd$  and  $\cos 2kd$  where  $k = \frac{2\pi}{\lambda}$  is the wavenumber and  $d$  is the displacement. The quantity  $\phi = 2kd$  is known as the total accumulated phase in the external cavity and is a measure of the optical path length (OPL).  $\phi$ , as opposed to distance, is the fundamental measured quantity in SMI and for this reason any perturbation to the effective wavelength in the cavity is inseparable from displacements by measuring the SMI signal alone. The general form of these modulations are given as the solutions to the set of non-linear equations

[4]

$$\begin{aligned} P_f &= P_0 \left( 1 + m \cos(\phi_f) \right) \\ \phi_0 &= \phi_f + C \sin[\phi_f + \arctan \alpha] \end{aligned} \quad (1)$$

where  $P$  is the optical power and  $\alpha$  is the linewidth enhancement factor. Here the subscript  $f$  denotes conditions subject to feedback while  $0$  denotes the free-running state of the laser.

By changing the position of the external reflector we induce both amplitude and frequency modulations in the internal laser cavity which can be measured by a photodetector. An important note is that this modulation is strongly periodic, repeating with every  $2\pi$  of accumulated phase. This gives rise to a "fringe" structure as shown in figure 1 B with each fringe corresponding to a displacement of  $\frac{\lambda}{2}$ .

In general, there are multiple solutions to the equations in 1. These solutions depend heavily on the value of the coupling parameter  $C$  which describes the strength of optical coupling between the internal and external cavities of the SMI system. The effect of this coupling is the generation of drastically different signal morphologies falling into one of several distinct regimes as shown in figure 10. These so-called coupling regimes arise due to the competition between oscillation modes within the compound laser system. When coupling is low, a single mode dominates and the feedback signal is a simple cosine of the accumulated phase. However, when coupling reaches a critical point ( $C=1$ ) the phase equations (1) admit 3 possible longitudinal modes within the external cavity. The laser system will tend to oscillate at the external cavity mode (XCM) with the lowest linewidth, however any slight perturbation in the external cavity length will induce mode-hopping between these possible XCMs [4]. The effect of this mode-hopping is hysteresis in the system's response to displacement which forms the characteristic discontinuities in the signal [3]. At very high coupling,  $C > 4.6$  the laser will enter a chaotic regime where it is multistable, leading to random mode-hopping and a loss of coherence. This regime is rarely useful for practical measurements.

The most important factor affecting this coupling is the intensity of the backscattered beam relative to that emitted by the laser. As can be seen in equation 1, the phase directly depends on this ratio  $\cos \phi_f = \frac{1}{m} \left( \frac{P_f}{P_0} - 1 \right)$

### A. State of the art

At the current state of the art, several issues with the most basic implementations of SMI have been observed. A significant fraction of the research in the SMI field has been towards relatively exotic methods of physical or algorithmic compensation in order to apply this technology to general-purpose measurements. In 2011, Donati reviewed these developments[5] and identified challenges including sensitivity of coupling to speckle and

target distance, laser wavelength instability, and the difficulty of finding suitable general-purpose DSP algorithms. Because the SMI signal morphology changes drastically with coupling and wavelength is a linear factor in the measurement, these issues greatly reduce the practical accuracy of SMI systems. Without corrections, SMI has very poor accuracy over large displacements, when measuring diffuse surfaces, in the presence of high-frequency vibrations, or environmental fluctuations. For this reason, SMI often requires manual in-place calibration of the setup and fine-tuning of processing algorithms before any measurements can be performed which limits the applicability of SMI as a commercial technology.

In literature, the coupling sensitivity issues have been approached using piezoactuated lenses [6] and online coupling control using liquid crystal attenuators [7]. These systems have the advantage of precise control over coupling so that the sensor be used over large motion ranges and on diffuse surfaces at the expense of complexity, cost, and more rigorous calibration. Further papers have explored multi-modal polarized gas laser sources for direct measurement of the frequency modulation [1] via heterodyne conversion at the photodetector. This gives additional information which can be used to improve the the displacement reconstruction while necessitating more advanced analog signal demodulation. Another important development was a method of obtaining absolute position measurements developed by [8] based on the principle of applying slight wavelength shifts to the laser source via pump current modulation.

### B. Algorithms

The selection of algorithms for SMI signal processing is another primary challenge of the technology. Given the vastly differing signal morphologies and applications of SMI there is no catch-all method for obtaining useful measurements from the photodetector signals. These algorithms come in several classes depending on the desired measurement. Processing algorithms exist for displacement reconstruction, as well as applications within vibrometry, velocimetry, and the measurement of laser properties.

The most common displacement reconstruction methods include simple fringe counting via gradient or multiscale edge methods, the wavelet transform [9], hilbert transform [10], and phase unwrapping [11]. This last method is the most promising by far since it is a direct approach to invert the laser feedback relations described by the LK equations. However this presents challenges of its own, specifically estimation of the coupling parameter  $C$  must be done online which in itself requires a separate class of optimization-based algorithms [12]. Measurement of laser properties such as linewidth enhancement factor is commonly done through the reconstruction of a known displacement and performing an iterative optimization [13] to minimize the error of the reconstruction

result.

Practical vibrometer and velocimeter solutions often use additional hardware to provide the requisite information. These include fringe-locking feedback loops [14] or bimodal polarized laser sources which directly read the doppler frequency shift via analog heterodyne conversion [2]. However, it is possible to perform either of these tasks via the simple SMI setup using displacement reconstruction methods or frequency analysis such as the Morlet wavelet transform [9] and FFT analysis[15].

### C. Detailed Physics

Given the wide range of SMI configurations available and physics that depend heavily on the laser source selected, we will focus here on semiconductor laser SMI. The definitive work describing the behaviour of semiconductor lasers subject to external feedback was developed by Lang and Kobayashi [3] and later extended by [16]. A full discussion of the field equations resulting from laser feedback provided by [3] are beyond the scope of this paper. Instead, we will attempt to identify all important parameters and practical effects of the system. The following equations pertain exclusively to semiconductor lasers operating well above their lasing threshold such that they exhibit a single longitudinal mode.

As discussed above, due to the external cavity formed between the laser emission mirror and the reflective target there exist many closely spaced XCMs. The possible XCMs are given by the solutions to phase equation 2 where  $\Delta\phi_L = n2\pi|n \in \mathbb{N}|$  [16].

$$\Delta\phi_L = \frac{\tau_L}{\tau_{ext}}(2\pi\tau_{ext}(\nu - \nu_{th}) + C \sin(d\pi\nu\tau_{ext} + \arctan\alpha)) \quad (2)$$

The coupling parameter C as introduced by [17] is defined by equation 3. It should be noted that many papers introduce varying notation here, for consistency we will follow the notation and form introduced by [18] and [16], equation 3.

$$C = \frac{d\eta_{ext}}{L\eta_{las}} \frac{\epsilon\sqrt{1+\alpha^2}}{\sqrt{A}} \frac{1-R}{R} \quad (3)$$

[16]

Where  $\epsilon \leq 1$  is the mode coupling efficiency typically taken as 0.5[18], R is the laser facet reflectivity, and  $A = \frac{P_e}{P_r}$  is the round-trip power attenuation of the back-reflected beam. Here L is the cavity length of the diode and n its refractive index.

In some papers, the ratio of optical path length (OPL) of the external and internal cavities is expressed in terms of flight time.

$$\frac{d\eta_{ext}}{L\eta_{las}} = \frac{\tau_e}{\tau_l} \quad (4)$$

From this it is clear that C will change linearly with distance to the target.

For  $C \ll 1$  equation 2 admits a single solution for the optical frequency  $\nu$  [16] and the returned amplitude signal is a simple cosine as described in equation 1 with the modulation coefficient m given by

$$m = A^{-1/2}[\frac{c}{2d}(\gamma - \frac{1}{\tau})] \quad (5)$$

generally on the order of 10E-3 for moderate feedback [18].

For  $C > 1$  the laser exhibits mode-hopping as described in detail by [3]. This multistability and hysteresis is possible due to the broad gain spectrum width and the dependence of gain and refractive index on carrier density in most semiconductor lasers. These effects as described by Lang and Kobayashi allow different longitudinal modes in the laser to be easily induced via external feedback conditions. For modelling and simulation of the SMI response we refer the reader to[4] and [12] which provides Matlab code for simulation.

Given the form of the phase equation for this system and the documented dependence of system dynamics on the coupling factor C it is clear that any external factors which affects these parameters introduce considerable errors in both signal morphology and displacement reconstruction accuracy. A practical interferometer must minimize these effects on the system's performance. The major environmental effects on the system are summarized as follows:

A change in diode pump current will change the refractive index of the gain medium[3] via changes to its temperature. In SMI with  $C > 1$  this effect can induce mode-hopping which is unrelated to target motion. In their testing, Lang and Kobayashi noted that the tendency to exhibit mode hopping with current variations was maximized when the external cavity length is an integer multiple of the the effective diode cavity. [3] (when the ratio in 4 is a whole number).

The temperature dependence of the gain medium refractive index in laser diodes can be practically approximated as linear.

$$n_{las} = n_0 + \frac{\partial n}{\partial T}T \quad (6)$$

With  $\frac{\partial n}{\partial T} \approx 5.5 \times 10^{-4}/K$  for GaAs [3].

This establishes a clear dependence of C on temperature since the effective laser cavity lengths depend on the refractive index of the medium. This is true for both the internal and the external cavity.

For an external cavity operating in air, the refractive index is given by Ciddor in [19]. The empirical correlations are lengthy and case-dependant so they will not be included here. In general the refractive index is a function of pressure, temperature, Co2 concentration, and air humidity. The refractive index is a parameter in the effective OPL of the external cavity. To gauge the sensitivity of n, a parameter study was performed using the

equations shown in [19] where the input parameters were individually varied through the ranges shown in table I. Parameters not varied were held at  $22^{\circ}\text{C}$ ,  $101.325\text{ kPa}$ ,  $50\%$  RH, and  $400\text{ ppm }x_{\text{CO}_2}$ . The calculations were done at a wavelength of  $640\text{ nm}$ . As can be seen from table I, the effects of temperature, pressure, and relative humidity have non-negligible effects and should be monitored, while the effects of carbon dioxide concentration can likely be ignored for general purposes.

Input	Range	Variation in $n$ [ppm]
Temperature	$18 - 20\text{ }^{\circ}\text{C}$	9.4
Pressure	$80 - 120\text{ kPa}$	106.5
Relative Humidity	0 – 100%	1
$\text{CO}_2$ Concentration	$400 - 1000\text{ ppm}$	0.08

Table I. Sensitivity Analysis of Refractive Index

The final effect on the system is that the gain profile of a diode laser will change with temperature and current density. Combined with the change in refractive index, the result of this is that the emission wavelength of a semiconductor laser will increase with the temperature of the diode and increasing current [20]. While the lasing wavelength response to temperature is a common feature of laser diode datasheets the current sensitivity is less commonly available. Fukuda et al. estimated the current coefficient to be on the order of  $0.008\text{nm/mA}$  when diode temperature was held constant. [20] It should be noted that the emission wavelength is quantized by the longitudinal mode spacing of the laser cavity according to

$$\Delta\omega = \frac{c}{2\eta L} \quad (7)$$

In summary, the above equations admit a set of parameters which must be controlled or calibrated for:

- A, power attenuation factor, the total optical losses experienced by the backscattered beam. This directly influences the coupling parameter and allows control via variable attenuators.
- $\frac{dn_{ext}}{Ln_{las}}$ , the ratio of external to diode cavity OPL. Coupling is directly proportional to this ratio and when close to an integer multiple it will drastically change the response to current/temperature fluctuations. This is affected by the laser diode temperature as well as the refractive index of the external cavity medium (typically air).
- $\lambda$ , the center wavelength. Given that displacement reconstruction requires the assumption of wavelength, control or knowledge of this directly affects reconstruction accuracy. The lasing wavelength is influenced by both diode temperature and pump current.

## II. SYSTEM DESIGN & CHARACTERIZATION

Here we discuss the design for a SMI system aimed to produce the lowest-cost displacement measurement setup with a maximum of configuration. We provide details of the characteristics and issues encountered with such an inexpensive system which closely match the physics described in section I C. A full component list for the critical components of the constructed system is given in table II and the completed system can be seen in figure 2.

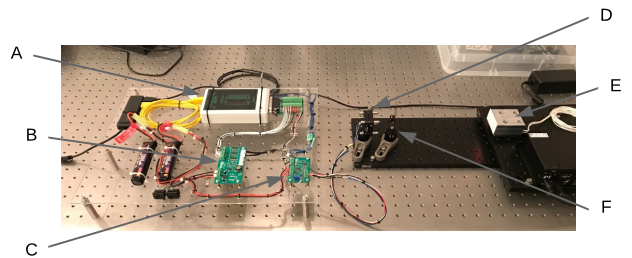


Figure 2. The constructed SMI system. A) USB-DUX Fast DAQ. B) Telemetry Amplifier Board. C) Laser driver and SMI signal amplification board. D) Collimation cage plate. E) Piezo stage with affixed retroreflective tape. F) ND filter.

### A. Optics

The optical design of the constructed SMI system was chosen to be as simple and inexpensive as possible. The selected laser diode was a HL6358MG with a nominal wavelength of  $639\text{nm}$ . It was chosen for its low cost and low-power operation while having the desired electrical configuration of the monitor photodiode (TO-can pin code A). Higher resolutions may be possible with shorter wavelengths, however as will be discussed in section II E the resolution is practically limited by the noise floor. A moulded glass aspheric lens was selected for collimation to avoid spherical aberration. The spot astigmatism did not present any issues in the operation of the system so it was left uncorrected. Semiconductor laser diodes typically have high divergence and astigmatism, as such the numerical aperture (NA) of the lens was selected to be sufficiently large for the divergence of the slow axis of the laser.  $\text{NA} > \sin(\theta_{max})$  During the initial testing of the system it was noted that a large  $5\text{mm}$  laser spot was less sensitive to misalignment on the tape retroreflector due to optical averaging over a greater surface. As such, a collimation lens with a large ( $f=11\text{mm}$ ) focal length was chosen. The large clear aperture of this lens also serves to maximize the amount of backscattered light re-entering the laser cavity as it is able to refocus a greater range of imperfectly reflected beams. This is important in SMI as any losses due to poor retroreflection will drastically reduce the effective optical coupling which may limit the

system to operating in the low-coupling regime.

For the target, a retroreflective CCR microprism tape was selected primarily due to cost. This method has the additional benefit of providing radial misalignment tolerance due to the fact that the retroreflective elements are tiled over a large surface. While a plane mirror or TIR prism retroreflector would provide excellent coupling, they must be carefully adjusted such that the reflection is not only parallel but also coaxial with the incident beam. The tape reflector was affixed to a PI precision piezo stage with 1nm resolution. This motion stage served as a ground truth reference for testing and calibration development.

Interchangeable ND filters were used to select the desired coupling regime. An important item of note is that the ND filter or attenuation method should be angled with respect to the beam to avoid formation of a tertiary resonator cavity as a result of reflections off the attenuator [1]. This may inject additional noise from vibrations of the attenuator. This could also be addressed with antireflective coatings, however the angling was observed to be very satisfactory in practice.

## B. Circuitry & Sensors

With the exception of applied science's[21] video on the topic, the authors were not able to find any detailed descriptions of the signal acquisition hardware used in current SMI research systems. In order to process the acquired SMI signal and provide requisite telemetry about the environment conditions several boards were developed and are provided open-source at [github.com/SMI](https://github.com/SMI). The components of the system are:

The data acquisition (DAQ) system selected was the USB-DUX Fast. This simple device is capable of sampling at up to 3MHz over 16 input channels. This allows for concurrent capture of all relevant data from the photodiode signal to the telemetry sensors without resorting to various sampling rates over multiple devices. Time synchronization of the received signals is then a trivial matter, and the high sampling rate allows the system to resolve fringes for rapidly moving targets. The low cost of this system and the direct python interface makes it ideal for capture in any kind of commercial application.

A transimpedance amplifier (TIA) is required to acquire a usable voltage signal from the photodiode current. The TIA must be tuned to the expected current of the photodiode and must be sufficiently high bandwidth to resolve high frequency structures in the signal. In order to provide adequate amplification of the SMI signal it must be highpassed using a cutoff frequency of 1Hz to remove the DC component which is several orders of magnitude larger than the desired modulation signal.

A highly stable constant current driver to avoid laser power fluctuations. This was designed using a precision voltage reference as shown in figure 3. The current driver can be tuned to the desired supply current using a trim-

mer pot. The laser drive current is given by the voltage across the resistor R1, and was designed for operation at 30mA with a ripple measured to be less than  $5\mu\text{A}$ .

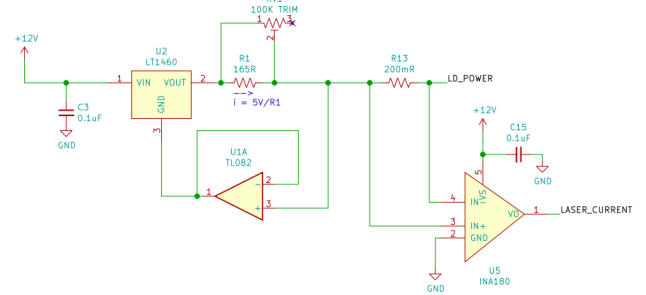


Figure 3. Laser constant current driver with current monitoring

The wavelength of a semiconductor laser is strongly dependent on its temperature and so this must be closely monitored. NB-PTCO-002 RTDs were selected to measure both diode and ambient temperatures for their exceptional linearity and very low noise. A whetstone bridge amplifier circuit was designed, balanced at room temperature, and provides a gain of several thousand to resolve minute changes in operating temperature. To achieve in-situ measurement of diode temperature, a miniature RTD was affixed to the back of the LD package using thermal epoxy. While the measured case temperature will be offset from that of the diode junction this can easily be addressed via a calibration. Additional RTDs and a pressure sensor were added to measure the ambient properties for calculation of the air refractive index.

## C. Issues

During construction and calibration of the system, a number of practical issues with this simple setup were observed.

The optical system encountered problems as a result of the inexpensive retroreflector selection. The microprism tape retroreflector solution has a power dropoff worse than the expected  $\sin(\theta_i)$  greatly limiting the allowable misalignment between the laser source and the target. As a result, coupling varied drastically with slight changes in angle as shown in figure 2. This was only partially mitigated by the large spot size discussed in section II A. It is recommended that a TIR retroreflector prism be used to solve this issue.

The designed circuitry lacked several features which would have increased the ease of use of the system. Firstly the feedback resistance of the TIA required careful calibration in order to achieve an appropriate gain while avoiding saturation of the OP-amp due to the large DC offset of the photodiode current. Since a high pass filter was only applied after the amplification step, the

unfiltered signal is not amplified sufficiently to provide the DC shift information required for complete phase-unwrapping. This can be addressed by implementing a voltage shift circuit instead of a high-pass for removal of the DC component. A schematic for implementation of this system using a microcontroller-generated voltage offset is provided in the supplementary materials.

The use of a pizeo-actuated motion stage as a motion reference introduced unique issues as compared to the speaker cones or piezo actuators used in literature. While the selected pizeo stage is incredibly precise (repeatable to 100nm), it utilizes a friction pusher mechanism which introduces undesirable vibrations and does not provide smooth motion. This sub-micron scale vibration creates significant sub-fringe structures in the signal as can be seen in figure 5 B. These "micro fringes" are the result of rapid direction change as the system vibrates. It should be emphasized that this is not noise, it is physical signal which matches the simulated response fairly closely. This was confirmed by comparing against a secondary motion reference which showed a total lack of these micro fringes. However, the use of this stage demands an exceedingly robust fringe detection method which can correctly determine between true noise and these fine structures.

#### D. Characterization

In order to analyze the performance of the system and establish the ability to control or calibrate for the parameters in section IC, characterization tests were performed. The most important of these were measurements of the noise floor, temporal drift, coupling response, and the system temperature response.

To evaluate the noise floor of the system, it was affixed to a vibration-isolating optical table and a signal was recorded at either end of a  $50\mu m$  displacement while the system was completely stationary. As shown in figure 5A, a power spectrum was computed using Welch's method.

To establish the temporal stability of the system, SMI signal for identical motion was collected and compared over a period of 24 hours. When overlayed as shown in figure 6, the signals show a small ( $< 1$  fringe) offset due to a difference in timing but little to no observable change in signal morphology. The system is relatively stable over this timeframe.

The coupling sensitivity of the system was characterized by installing a fixed ND filter with an OD of 0.3 and commanding a motion of several mm using the precision stage. By the Lang and Kobyashi equations, it is expected that coupling strength should be a linear function of distance to the target. To evaluate whether this was indeed the case for our device, a 2mm out-and-back motion was recorded and is shown in figure 7. The fringe amplitude (and therefore coupling of laser light back into the cavity) changes roughly linearly with distance, however there are severe oscillations. A possible explanation

of this variation is the speckle phenomenon which is likely present due to the high scattering of light from the many elements retroreflector tape.

Using the RTD sensor applied to the back of the laser diode, an experiment in temperature response was performed. The diode was heated and the ambient temperature was held constant to isolate the effects of diode temperature on lasing wavelength. Signals were collected using a precision motion stage to move a known distance. The number of fringes detected were plotted as a function of temperature, as shown in figure 8. The fringe count changes linearly in accordance to the linear increase in wavelength expected from IC. This measurement suggests that a simplistic temperature calibration is possible for this system without necessitating active temperature control.

#### E. Limitations

Beyond the encountered issues, the constructed system has several inherent limitations. The most egregious of these is that the coupling control via ND filters is a manual process with fairly coarse steps between available filter densities. This required the system to be essentially calibrated in place for each measurement and did not allow for fine-tuning of the coupling regime. This effectively limits the maximum displacement range of the sensor to at best 1-2mm before the signal morphology is excessively altered. While it may be possible to overcome this with matched filter methods that adapt to the changing fringe structure over time this is a fundamental challenge of any SMI system which does not have active coupling control.

A more fundamental limitation of the system is the maximum resolvable velocity. This is directly proportional to the sampling rate available since a fringe will occur at every  $\frac{\lambda}{2}$ . Applying the Nyquist criterion, the maximal velocity,  $v$ , for a given sampling rate is given by equation 8.

$$\frac{F_s}{2} = \frac{2v}{\lambda} \quad (8)$$

For our system which is able to sample at up to 1MHz the theoretical maximum is approximately 0.6m/s. However in practice it was observed that in order to appropriately sample the discontinuities we needed to exceed the Nyquist criterion by 5x, setting a practical upper bound at 0.13m/s. Furthermore, the maximum range of the sensor is limited by the coherence length of the laser. To ensure coherence at the laser source, the OPL of the external cavity must be less than half the coherence length due to the out-and back path taken. This requirement restricts the range of any self-mixing system, however even diode lasers with typically large FWHM linewidths are sufficient for a wide range of practical measurements.

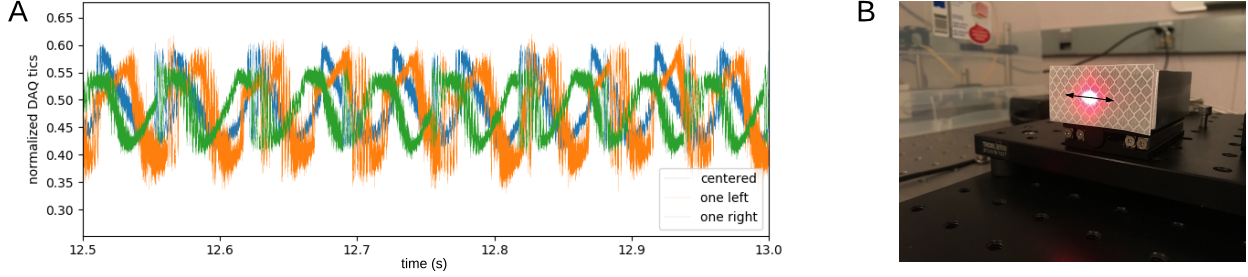


Figure 4. Effect of moving the laser around on the retro-reflective tape on signal morphology.

### III. A PRACTICAL APPLICATION: THE QUANTUM SWITCH

Given the challenges in the measurement of macro-scale motions while retaining a simple and low-cost hardware configuration it would be highly advantageous to focus on the other strengths observed. Given the periodic nature of the signal and the discontinuities present at each fringe in the medium coupling regime, it was hypothesized that a system initialized very near to one of these discontinuities should be able to obtain exceptional sensitivity as was discussed by [14].

The detected amplitude signal has the form given by equation 1 and is a cosine of the accumulated phase,  $\phi = 2kd$  which has a maximum sensitivity when  $\phi = \pi/2$  given by equation 9 [14].

$$(\Delta I/I_0)^2 = \phi^2 \quad (9)$$

While the resolution of the conventional interferometry system inherently requires a robust displacement reconstruction method to be meaningful, this "quantum switch" could operate by simply observing the level change in the signal and resolve displacements on the order of 10nm. This method of measurement allows the system to operate at close to the quantum noise limit.

Applying equation 10 proposed by Donati in [14] which we can compute the noise equivalent displacement of the system based on the SNR with respect to shot noise on the photodiode current measurement. The shot noise is given by  $\Delta I = 2eI_0B$  where B is the bandwidth and I is the photodiode current.

$$NED = \frac{\lambda}{2\pi\sqrt{eBI_0}} = \frac{\lambda}{4\pi\sqrt{SNR}} \quad (10)$$

Using the approximate SNR of 10 measured from the amplified signal observed in practical use the NED can be estimated at  $\approx 16$ nm. With improved vibration isolation and more optimized electrical hardware with a lower bandwidth this could likely be substantially improved down into the single digit nm or even picometer range as suggested by [14].

With fairly minimal effort towards biasing the system close to the half-fringe point, the constructed was able to consistently resolve an out-and-back motion of 25nm as shown in figure 9. At this scale, the SNR is fairly low but considering the cost of the system this is an impressive result. Based on this experience, the 10-15nm range is likely a practical bound for this simplistic SMI setup.

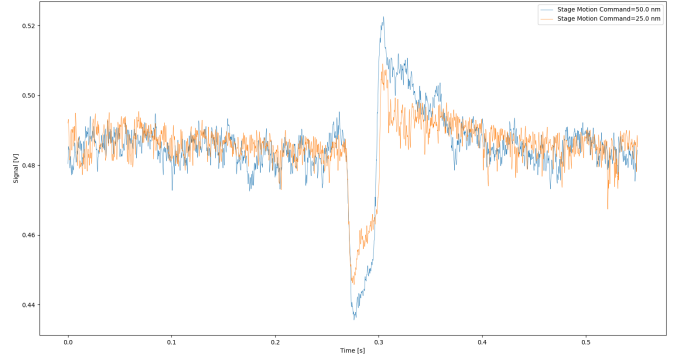


Figure 9. Experimental SMI signals captured for 50nm and 25nm motions

This "quantum switch" application may be useful in a variety of nano-sensing systems. It has the advantage of being an order of magnitude less expensive than conventional Fabry-Perot interferometers and nano-capacitive sensors of similar resolution. The measurement is non-contact and can be extended to ranges well in excess of those available using common capacitive sensing. These specific advantages could allow SMI to compete in multi-sensor configurations or where direct integration into active systems is required. SMI also has the potential advantage of a remote sensor head via fiber-optic coupling, allowing extremely low-profile and minimally invasive measurements. This advantage could be crucial in environments with high radiation or magnetic fields such as within a nuclear reactor or MRI.

Half-fringe locked SMI is of specific interest in vibrometry [14] since it allows the resolution of nano-scale vibrations at very high frequencies. These systems can

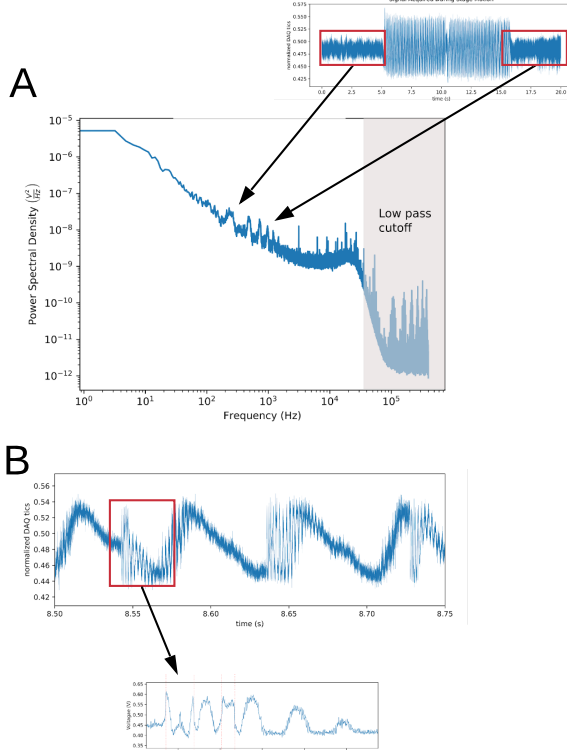


Figure 5. Analysis of the additive and structured noises observed in the signal. A) Power spectrum of the additive noise constructed using Welch's method [22]. It is approximately  $1/f$ , as typical for semiconductor devices. B) Close up on the structured noise. It can be seen to be composed of fringes at a much higher frequency than the main signal. These high-frequency fringes were found to be due to mechanical vibrations induced by the motion stage.

also be integrated directly into optical systems to provide deflection and pointing drift measurements in satellites, telescopes and high-power laser applications. Current applications for nanoscale sensing include nano positioning feedback control, silicon wafer and lithography mask inspection, beamline alignment in synchrotrons, and atomic force microscopy. These applications currently all use high cost piezoelectric, capacitive, or interferometric sensing [23] which may be either augmented or replaced by SMI-based systems.

#### IV. CONCLUSIONS

Through design and characterization of a basic SMI setup, we have demonstrated and described the practical issues inherent to such a simple system. We have conducted a review of all practical considerations involved in the development and specification of such a system and provided an open-source hardware solution to allow signal

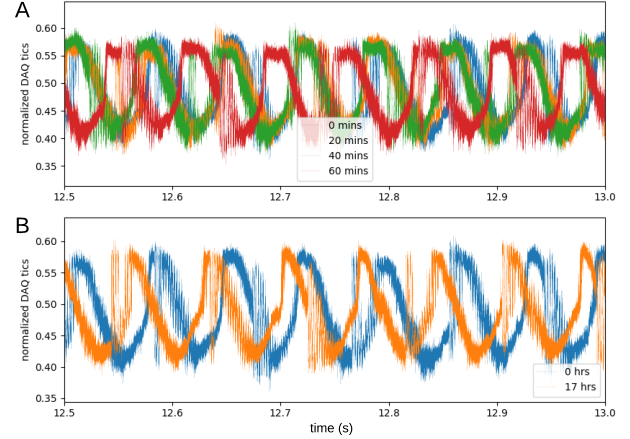


Figure 6. Fringes observed over the course of an hour (A) and a day (B). Fringe morphology does not noticeably change.

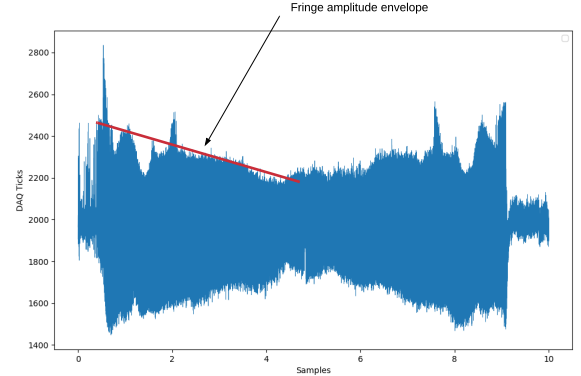


Figure 7. Signal recorded from a 2mm out-and-back motion.

acquisition for general SMI systems.

The lack of control over coupling and temperature instability was found to complicate the development of an accurate long-range displacement reconstruction algorithm. In this paper, we have demonstrated an alternate application for SMI to nano-scale measurements which can circumvent the majority of these challenges.

The total BOM cost of our sensor using exclusively off-the-shelf components was \$309 USD. By substituting comparable low-cost plastic lenses and a simplistic fixed collimation assembly, this could be brought down below \$200 even at low-volume purchase prices. This is easily an order of magnitude less than capacitive sensors, and 3 orders of magnitude better than commercial interferometers.

To compare our device against similar sensors of different technologies we selected Micro-Epsilon's CS005 capacitive distance sensor, the Renishaw RLD10+REE400 differential interferometer, and the SP 5000 NG Fabry-

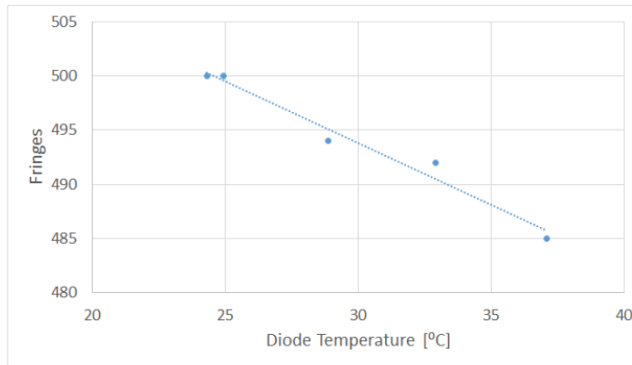


Figure 8. Number of fringes as a function of diode temperature.

Perot interferometer. This comparison is shown in table III. Quite clearly SMI cannot compete on resolution or accuracy with high-price interferometry instruments. However it is quite competitive with capacitive sensors and handily beats them on price and operational range. This suggests that inexpensive SMI sensors may be best suited to replace capacitive sensors in nano-sensing applications as compared to general interferometry applications. These sensors should be able to achieve resolution on the order of 10nm with accuracy in the low PPM using environmental calibrations developed based on the characterizations presented herein.

- 
- [1] S. Donati, “Laser interferometry by induced modulation of cavity field,” *Journal of Applied Physics*, vol. 49, no. 2, p. 495–497, 1978.
- [2] M. J. Rudd, “A laser doppler velocimeter employing the laser as a mixer-oscillator,” *Journal of Physics E: Scientific Instruments*, vol. 1, no. 7, p. 723–726, 1968.
- [3] R. Lang and K. Kobayashi, “External optical feedback effects on semiconductor injection laser properties,” *IEEE Journal of Quantum Electronics*, vol. 16, no. 3, pp. 347–355, 1980.
- [4] G. Plantier, C. Bes, and T. Bosch, “Behavioral model of a self-mixing laser diode sensor,” *IEEE Journal of Quantum Electronics*, vol. 41, no. 9, pp. 1157–1167, 2005.
- [5] S. Donati, “Developing self-mixing interferometry for instrumentation and measurements,” *Laser & Photonics Reviews*, vol. 6, no. 3, p. 393–417, 2011.
- [6] M. Norgia, S. Donati, and D. D’Alessandro, “Interferometric measurements of displacement on a diffusing target by a speckle tracking technique,” *IEEE Journal of Quantum Electronics*, vol. 37, no. 6, pp. 800–806, 2001.
- [7] M. Norgia and S. Donati, “A displacement-measuring instrument utilizing self-mixing interferometry,” *Instrumentation and Measurement, IEEE Transactions on*, vol. 52, pp. 1765 – 1770, 01 2004.
- [8] F. Gouaux, N. Servagent, and T. Bosch, “Absolute distance measurement with an optical feedback interferometer,” *Appl. Opt.*, vol. 37, no. 28, pp. 6684–6689, Oct. [Online]. Available: <http://ao.osa.org/abstract.cfm?URI=ao-37-28-6684>
- [9] J. Perchoux, A. Quothb, R. Atashkhooei, F. Azcona, E. Ramírez-Miquet, O. Bernal, A. Jha, A. Luna-Arriaga, C. Yanez, J. Caum, and et al., “Current developments on optical feedback interferometry as an all-optical sensor for biomedical applications,” *Sensors*, vol. 16, no. 5, p. 694, 2016.
- [10] Z. Zhang, C. Li, and Z. Huang, “Vibration measurement based on multiple hilbert transform for self-mixing interferometry,” *Optics Communications*, vol. 436, p. 192–196, 2019.
- [11] S. Merlo and S. Donati, “Reconstruction of displacement waveforms with a single-channel laser-diode feedback interferometer,” *IEEE Journal of Quantum Electronics*, vol. 33, no. 4, pp. 527–531, 1997.
- [12] Y. Fan, Y. Yu, J. Xi, and J. F. Chicharo, “Improving the measurement performance for a self-mixing interferometry-based displacement sensing system,” *Appl. Opt.*, vol. 50, no. 26, pp. 5064–5072, Sep 2011. [Online]. Available: <http://ao.osa.org/abstract.cfm?URI=ao-50-26-5064>
- [13] Y. Gao, Y. Yu, J. Xi, Q. Guo, J. Tong, and S. Tong, “Improved method for estimation of multiple parameters in self-mixing interferometry,” *Appl. Opt.*, vol. 54, no. 10, pp. 2703–2709, Apr 2015. [Online]. Available: <http://ao.osa.org/abstract.cfm?URI=ao-54-10-2703>
- [14] S. Donati and M. Norgia, “Overview of self-mixing interferometer applications to mechanical engineering,” *Optical Engineering*, vol. 57, no. 05, p. 1, Jan 2018.
- [15] M. Wang, “Fourier transform method for self-mixing interference signal analysis,” *Optics and Laser Technology*, vol. 33, no. 6, p. 409–416, 2001.
- [16] K. Petermann, “External optical feedback phenomena in semiconductor lasers,” *IEEE Journal of Selected Topics in Quantum Electronics*, vol. 1, no. 2, p. 480–489, 1995.
- [17] G. Acket, D. Lenstra, A. D. Boef, and B. Verbeek, “The influence of feedback intensity on longitudinal mode properties and optical noise in index-guided semiconductor lasers,” *IEEE Journal of Quantum Electronics*, vol. 20, no. 10, p. 1163–1169, 1984.
- [18] G. Giuliani, S. Bozzi-Pietra, and S. Donati, “Self-mixing laser diode vibrometer,” *Measurement Science and Technology*, vol. 14, no. 1, p. 24–32, 2002.
- [19] P. E. Ciddor, “Refractive index of air: new equations for the visible and near infrared,” *Applied Optics*, vol. 35, no. 9, p. 1566, 1996.
- [20] M. Fukuda, T. Mishima, N. Nakayama, and T. Masuda, “Temperature and current coefficients of lasing wavelength in tunable diode laser spectroscopy,” *Tdls 2009*, p. 145–150, 2011.
- [21] “Laser diode self-mixing: Range-finding and sub-micron vibration measurement, howpublished = <https://www.youtube.com/watch?v=mudro-6u2zg>, author = Ben Krasnow.”
- [22] M. H. Hayes, *Statistical Digital Signal Processing and Modeling*, 1st ed. USA: John Wiley & Sons, Inc., 1996.
- [23] F. J. Giessibl, “Advances in atomic force microscopy,” *Reviews of Modern Physics*, vol. 75, no. 3, p. 949–983,

2003.

### Appendix A: Component List

Component	Price	Supplier
HL6358mg Laser diode	17	Thorlabs
C22TMD-A Aspheric Lens	80?	Thorlabs
LDH56-P2 Collimation Cage Plate	120	Thorlabs
BRT-THG-1-100 Retroreflective tape	43	Banner
Q-545 Piezo Stage	5000	PI
E873 Motion Controller	1000	PI
USB-Dux Fast DAQ	200	USB-DUX
NB-PTCO-002 RTD	30	Digi-Key

Table II. Components of the constructed system

	Fabry-Perot (SP5000NG)	SMI	Capacitive (CS005)	Differential (RLD10)
Resolution [nm]	0.005	0.6	0.5	0.395
Accuracy [nm]	5	100	200	2.5
Range [m]	5	1	0.01	4
Price (est.)	20000	200	3000	15000

Table III. Comparison to commercial precision distance sensors

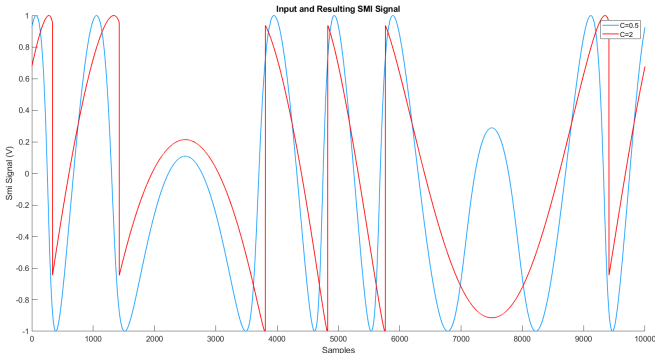


Figure 10. Simulated SMI signals for low ( $C=0.5$ ) and moderate ( $C=2$ ) coupling regimes

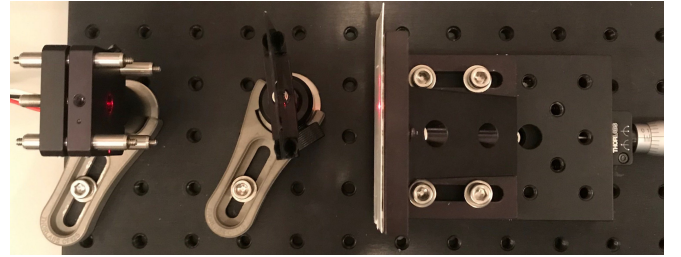


Figure 11. Optics Setup Detail

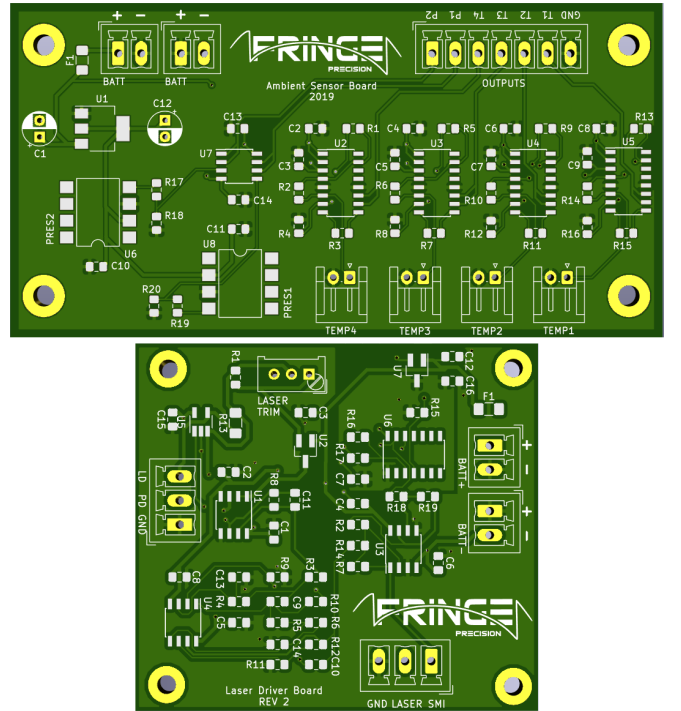


Figure 12. Sensor and laser driver custom PCBs.

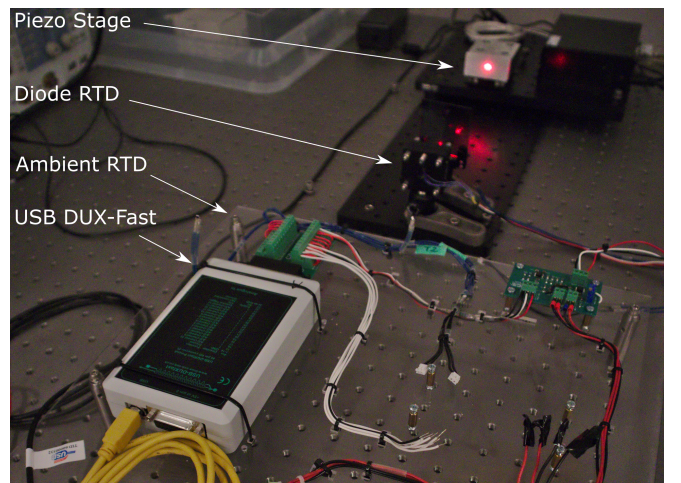


Figure 13. System overview showing DAQ layout and motion stage target